CIVIL ENGINEERING JOURNAL

Article no. 22

THE CIVIL ENGINEERING JOURNAL 3-2024

DETECTION METHOD OF TUNNEL SURROUNDING ROCK LEAKAGE CHANNEL BASED ON IMPROVED CHAOTIC PARTICLE SWARM OPTIMIZATION ALGORITHM

Lei Zhu[1], Peixuan Qiao, Fuyu Jiang[3] , Caihua Shen[3], Yuke Jiang[1]

1. *Zhongjiao Tunnel Bridge (Nanjing) Technology Co., Ltd., Jiangsu, Nanjing, 211800, China*
2. *Anhui Water Resources and Hydropower Survey and Design Research Institute Co., Ltd., Hefei, Anhui, 230088, China, huandengwoqiao2@163.com*
3. *School of Civil Engineering and Transportation, Hohai University, Nanjing, Jiangsu, 210098, China*

ABSTRACT

Leakage channels in tunnel lining and surrounding rock can lead to water seepage on tunnel walls, significantly posing risks to the safety and stability of tunnel operations. Accurate detection of these leakage channels is important to block them and maintain safe operations of tunnels. Based on the theory of natural potential field detection, the potential distribution on the tunnel wall is studied. An improved particle swarm optimization algorithm is applied to invert the spatial charge distribution inside the tunnel lining and surrounding rock. The distribution of spatial charges is used to infer the location and direction of leakage channels within the tunnel lining and surrounding rock. The research results show that the variance of charge distribution is 1.58% in the forward modeling inversion and 7.6% in the inversion of measured data. The inverted result shows an area of charge anomaly consistent with the actual position of the leakage channel.

KEY WORDS

Spontaneous potential method, Particle swarm optimization, Coupling of multiple physical fields, Tunnel seepage

INTRODUCTION

Water seepage in the tunnel wall will affect the normal operation and lifespan of tunnel electromechanical equipment, leading to cracking or detachment of t tunnel lining, posing a threat to tunnel stability. In China, tunnel leakage is a significant issue. In 1995, a survey of 4855 railway tunnels revealed that 1428 tunnels had severe leakage, accounting for 29.4% of the total. According to the statistics of China's railway tunnel technical status in 1997, there were more than 5,000 railway tunnels in operation along the entire line. Among them, about 70% of the tunnels have leakages, and 1,502 tunnels were affected by cracking and water leakage, accounting for more than 30% of the total railway tunnels [1-2]. One of the main causes of these diseases is that the groundwater flows through the seepage channels in the surrounding rock and soil mass of the tunnel, continuously eroding the tunnel lining layer, leading to the breakage of the tunnel lining layer. The location detection of tunnel leakage channels has always been a challenging engineering problem. In practice, the method of repairing the leakage channel mostly adopts extensive excavation and then filling, which is blind, ineffective and wasteful. Therefore, it is necessary to detect the leakage channels

DOI 10.14311/CEJ.2024.03.0022

inside the tunnel lining and surrounding rock and to repair the leakage channels according to the detection results.

According to the flow potential effect, uneven distribution of positive and negative charges will occur in the leakage channel, causing abnormal distribution of potentials in the inner wall of the tunnel. In line with the principle of natural potential method exploration, it is possible to use the distribution of potentials in the inner wall of the tunnel as a known condition to detect the internal distribution of electric charges in the tunnel surrounding rock [3-5]. This article will study the detection method for the location of tunnel surrounding rock leakage channels based on the principles of flow potential effect and natural electrical exploration, striving to provide direction for the management of tunnel leakage water sections.

MATERIALS AND METHODS

Study on Forward Modeling of Electric Potential Distribution on Tunnel Walls

The essence of the abnormal distribution of natural electric field on the tunnel lining's inner wall is the selective adsorption of charged particles in the liquid by the surrounding rock and lining layers, leading to the directional separation of charged particles. This abnormal distribution of natural electric field is coupled with the seepage field, and there is a coupling relationship equation between the seepage field and the natural electric field under saturated conditions [6-8]. Under quasi-static conditions, the total current density $j$in saturated porous media can be represented as follows:

$$j = -\sigma_{sat} \nabla \varphi + j_s \tag{1}$$

where φ, σ_{sat} and j_s are the potential, conductivity and flow current density, respectively. Under saturation conditions, the flow current density j_s is expressed asfollows:

$$j_s = \sigma_{sat} C_{sat} \nabla P \tag{2}$$

where σ_{sat} is the conductivity of the pore water under saturated conditions; C_{sat} is the coupling coefficient of the flow potential under saturated conditions, and P is the pressure. Charge is conserved under quasi-static conditions, and the equation can be calculated as follows:

$$\nabla \cdot j = 0 \tag{3}$$

The governing equations of the flow potential can be obtained from Eqs.(1) and (3):

$$\nabla \cdot \sigma_{sat} \nabla \varphi = \nabla \cdot j_s \tag{4}$$

The coupled relationship equations between the seepage field and the natural electric field in the saturated state can be obtained by coupling Equatios (2) and (4):

$$\nabla \cdot \sigma_{sat} \nabla \varphi = \nabla \cdot \sigma_{sat} C_{sat} \nabla P \tag{5}$$

Based on the above analysis, a three-dimensional coupled seepage field-natural electric field model is established within the Comsol multi-physics software for the analysis of the potential distribution on the inner wall of the tunnel. The model is shown in Figure 1. The boundary condition used for the model is the Delicacy boundary condition with a value of 0 at infinity.

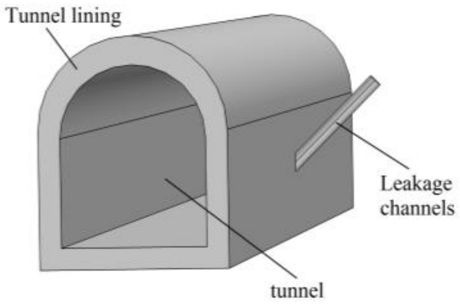

Fig. 1 - Schematic diagram of tunnel forward model

According to theoretical analysis, the low water pressure appears at the location of the leakage channel. Due to the variation of water pressure, the flow velocity and direction at the location of the leakage channel also change [9-11]. Based on the coupled relationship between the natural electric field and seepage field (Equation 5), the electric potential distribution at the leakage channel location can be calculated. It can be seen from Figure 2 that there is an obvious positive potential feature close to the inner wall of the tunnel, and a significant negative potential feature at a position away from the inner wall of the tunnel. Figure 3 illustrates the electric potential distribution on the tunnel walls.

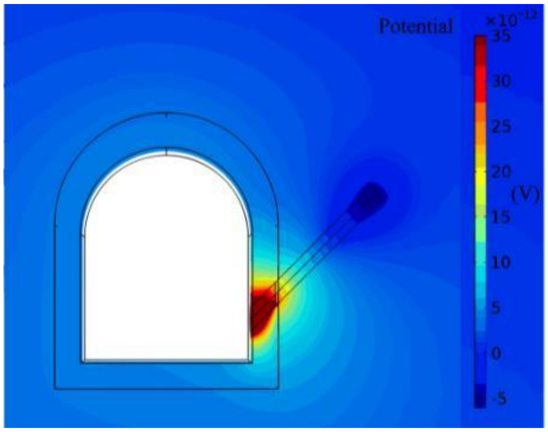

Fig. 2 - Potential distribution diagram of leakage channel position

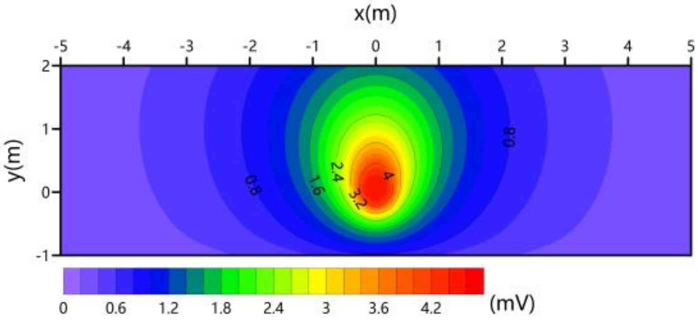

Fig. 3 - Potential distribution of inner wall of tunnel

DOI 10.14311/CEJ.2024.03.0022

Inverse study of charge distribution in tunnel surrounding rock

In the inversion of the space charge distribution, the inversion can be divided into the following three steps:

① Construct the fitness function;

② Solve the solution when the fitness function takes the minimum value;

③ Output of results and graphical display;

In inversion, the establishment of the fitness function is the most important part, and the construction of fitness function can be divided into the following steps:

(1) Randomly generate *n* points in the target inversion space, with the positions (x_i, y_i, z_i)and the charges of the point as q_i, where $i = 1, 2, 3 .....n$.

(2) Import the measured data. The position and potential of each point in the measured data is(x_j, y_j, z_j) and U_j, where $j = 1, 2, 3 .....m$, *m* is the number of measured data points.

(3) The sum potential U_{merj} generated by all point charges in space at the location of the *jth* real point can be expressed as follows:

$$U_{merj} = \sum_{i=1}^{n} k \frac{q_i}{r_{ij}^2} \tag{6}$$

where *k* is the Coulomb constant, q_i is the charge of the *i-th* point charge, and r_{ij} is the distance from the *i-th* point charge to the *j-th* data point.

(4) Use V_j as a parameter to measure the deviation between the measured potential at the location of the *j*-th data point and the combined potential U_{merj}, V_j is expressed as follows:

$$V_j=\left|\frac{U_{merj}-U_j}{U_j}\right| \tag{7}$$

(5) The average deviation $\overline{V_a}$ from the measured value of the combined potential generated by all point charges in space at all measured point positions is as follows:

$$\overline{V_a} = \frac{\sum_{j=1}^{m} V_j}{m} \tag{8}$$

Construct the fitness function f_{ad} as follows:

$$f_{ad}=\overline{V_a} \tag{9}$$

f_{ad} is a function of x_i, y_i, z_i, q_i.

Taking x_i, y_i, z_i and q_i as the unknowns of the fitness function f_{ad} for solution when the fitness function f_{ad} is minimized, these solutions can represent the position and charge of each point, and $i = 1, 2, 3 ...n$. Since the fitness function may be underdetermined and unknowns are large, it is solved using a nonlinear optimization algorithm.

The particle swarm optimization algorithm is an evolutionary algorithm inspired by bird flocking behavior, and developed by Kennedy and Eberhart [12], and El Rassy et al. [13]. Particle swarm algorithm is an iterative optimization algorithm that firstly creates a set of random solutions in the solution space, i.e. the initial particle swarm. Then it takes the optimal solution in the initial particle swarm, allowing the remaining particles to follow the optimal particles for optimization in the solution space, and gradually approach to the better solution by adjusting the particle's moving speed and position [14-15].

The solution of the above fitness function belongs to the solution of multi-dimensional and multi-peak function. As can be seen from the previous studies [16-18], compared with other nonlinear solution methods, the particle swarm algorithm for multi-dimensional, multi-peak problems has the advantages of strong solving ability, good convergence, good stability, high computational efficiency, and simple parameters, which is very suitable for the solution of the minimum value of the above fitness function. In this study, the particle swarm algorithm is used to solve the solution when the fitness function takes the minimum value.

Improvements to the Particle Swarm Optimization (PSO)

Traditional PSO-based inversion algorithms has problems such as easy to fall into the local optimal solutions, the multiple solutions leads to mismatch between the inversion results and the actual situation, and difficulty in displaying the inversion results are difficult to display. In response to the above problems, the PSO-based inversion algorithm is improved.

Adaptive Weight Method

In a traditional PSO algorithm, the inertia weight is a fixed value, typically between 0.4 and 0.9. A smaller inertia weight will weaken the global search capability of the PSO algorithm, while a larger one will weaken its local improvement ability [19-21]. To balance the global search and local improvement capabilities of the PSO algorithm, a nonlinear dynamic inertia weight coefficient formula can be expressed as follows (10):

$$\omega = \begin{cases} \omega_{min} - (\omega_{max} - \omega_{\min}) \times (f - f_{min})\left(f_{avg} - f_{min}\right), f \leq f_{avg} \\ \omega_{max}, f > f_{avg} \end{cases} \tag{10}$$

where $\omega_{max}$and ω_{min} are the maximum and minimum values of ω, respectively f is the current fitness of the particle; f_{avg} are the average fitness of all current particles, and $f_{min}$is the minimum fitness of all current particles.

In the above equation, the inertia weight will automatically change with the objective function value of the particle, is hence called the adaptive weight [22-24].

When the objective value of each particle tends to be consistent or tends to be locally optimal it will increase the inertia weight; while when the objective value of each particle is more dispersed, it will decrease the inertia weight. Meanwhile, for particles whose objective function values are better than the average objective values, the corresponding inertia weight factor is smaller, protecting the particles. On the other hand, for particles whose objective function values worse than the average objective values, the corresponding inertia weight factor is larger, making the particles closer to the better search area.

Chaos Mapping Method

When the PSO algorithm iterates to a certain extent, the traditional PSO algorithm is prone to getting stuck in local optima and unable to escape. When the PSO algorithm falls into a local optimum, if it can force some particles to break through the local optimum and continue global search, it can significantly improve the global search ability of the PSO algorithm.

Chaos is a widespread nonlinear phenomenon in nature. It may seem chaotic, but it has a complex internal structure, featuring randomness, ergodicity, and regularity. It is highly sensitive to initial conditions and can traverse all states within a certain range without repetition according to its own rules. Based on the properties of chaotic motion, optimization searches can be carried out [25-26]. The main idea of introducing chaotic optimization search techniques into the PSO algorithm is to incorporate the computation process of the PSO algorithm the main procedure. When the optimal fitness of the population changes very little in *n* iterations, indicating that it has fallen into local optima, chaotic optimization search is applied to particles with the optimal fitness. This drives the particle to escape the local optimum, thereby improving the trend of PSO algorithm falling into local optima in the later stages of evolution [27-29].

To improve computational efficiency, chaotic optimization search is not triggered in the early stages of evolution due to the fast convergence speed of PSO algorithm. However, in the later stages, when the convergence of the PSO algorithm slows down, chaotic optimization search will be called multiple times for optimization.

The chaos mapping method used in this study is the Logistic-Sine-Cosine chaotic mapping, and the formula to generate chaotic sequences is as follows (11):

$$y_{i+1} = \cos\{\pi[4ry_i(1-y_i) + (1-r)sin(\pi y_i) - 0.5]\}, r \in [0,1] \tag{11}$$

where y_1 is a random number; y_2—y_{i+1} is generated by the chaos mapping formula, and y_1-y_i is the chaos mapping sequence.

The chaotic sequence is mapped into the x_i-centered domain by carrier wave, and expressed as follows (12):

$$x_i^{'} = x_i + R(2y_i - 1) \tag{12}$$

where R is the chaotic search radius, and the value range of $x_i^{'}$ is as follows:

$$x_i^{'} \in [x_i - R, x_i + R] \tag{13}$$

The update formula for particle swarm velocity is as follows:

$$\mathrm{v}_i^{'} = \frac{x_i^{'} - x_i}{\|x_i^{'} - x_i\|} \tag{14}$$

Adaptive Outlier Filtering Method

When applying the traditional PSO algorithm to the inversion of leakage channels within the tunnel lining and surrounding rock in a three-dimensional space, the reliability of the inversion results will be inevitably affected by the multiple solutions. On one hand, the inversion results may significantly deviate from reality; on the other hand, the results from two different inversions may be entirely dissimilar. To address this issue, constraints need to be applied to the inversion process and results.

According to the basic geological distribution pattern, the distribution of charges is continuous and smooth, and it is unlikely that there will be a sudden change in charges. Therefore, this regularity can serve as a constraint to eliminate mutation points, reduce the existence of multiple solutions, and make the inversion results closer to reality.

To eliminate mutation points, this inversion algorithm adopts an outlier determination-correcting method based on the Pautacriterion to rectify mutation points. During the correction process, an adaptive weighting coefficient δ is introduced to avoid data distortion and overcorrection.

The calculation steps are as follows:

(1) Calculate the distance r_{km} from the data point *k* to all remaining data points in the solution space, where *k = 1,2,3... n*， *m=1,2,3... n*, and *n* is the total number of points in the group.

(2) The sphere with the radius *R* is determined with the data point *k* as the center.

(3) When the number of points with a distance to the data point *k* less than *R* is greater than *l*, the standard deviation and average value of all points in the sphere range with *R* as the radius are obtained. The value of the data point *k* is corrected according to Eq. (15) when the difference between the value of the data point *k* and the average of all points in the range is greater than *q* times the standard deviation; otherwise, the value of the data point *k*(val_k) remains unchanged.

$$val_k = \sum_{i=1}^{n} \frac{r_{ki}}{\sum_{j=1}^{n} r_{kj}} \times val_i \times (1-\delta) + val_k \times \delta, i = 1,2,3 \cdots s, j = 1,2,3 \cdots s, k = 1,2,3 \cdots n \tag{15}$$

where *s* is the number of all points in the range except the data point *k*; val_i is the amount of charge of the data point *i*; r_{kj} and r_{ki} are the distance between data point *k* and data points *i* and *j*. The coefficient δ is determined as follows:

$$\delta = 1.2^{-(s-1)} \tag{16}$$

(4) When the number of points whose distance to the data point *k* is less than *R* is less than or equal to *l*, the standard deviation and the mean of these *l* points plus data point *k* are sought. The data point *k* is corrected according to Equation (17) when the difference between the data point *k* and the average of the sought *l+1* points is greater than *q* times the standard deviation; otherwise, the value of the data point *k* remains unchanged.

$$val_k = \sum_{i=1}^{n} \frac{r_{ki}}{\sum_{j=1}^{n} r_{kj}} \times val_i \times (1-\delta) + val_k \times \delta, i = 1,2,3 \cdots l, j = 1,2,3 \cdots l, k = 1,2,3 \cdots n \tag{17}$$

where val_i is the amount of charge of the data point; r_{kj} and r_{ki} are the distance between the data point *k* and data points *i* and *j*. The coefficient δ is determined as follows:

$$\delta = 1.2^{-(l-1)} \tag{18}$$

Four-Dimensional Discrete Data Point Grid Interpolation Method

In the inversion of leakage channels within the tunnel lining and surrounding rock in three-dimensional space, the output result of the PSO algorithm is represented as an$n$×4matrix.In the output matrix, the first three columns are the position of the data point, and the fourth column is the charge of the point val_i, i=1,2,3…n. As the data points in the output result are sparsely distributed in three-dimensional space, it is challenging to visualize them directly. To address this, a four-dimensional discrete data point grid interpolation algorithm is designed to visualize the randomly distributed four-dimensional data points. The algorithm steps are as follows:

(1) Establish a uniformly distributed three-dimensional grid of pointsp_j, and set the charge corresponding to each three-dimensional grid point as$dval_j$, where$j = 1,2,3 \ldots m$, and m is the number of three-dimensional grid points.

(2) Calculate the distance from all date points to the three-dimensional grid point p_j and indicate them by r_1, r_2, r_3…r_n. In addition, when r_i is 0, r_i is changedto1.0×10^{-100};

(3) Calculate the weight of all date points to 3D mesh point p_j according to Eq. (19), $j = 1,2,3 \ldots m$:

$$weight_i = \frac{r_i}{\sum_{i=1}^{n} r_i}, i = 1,2,3 \ldots n, \tag{19}$$

(4) Calculate the charge amount $dval_j$ of the three-dimensional grid point $p_j$as follows:

$$dval_j = \sum_{i=1}^{n} weight_i \times val_i, i = 1,2,3 \ldots n, j = 1,2,3 \ldots m, \tag{20}$$

(5) The coordinates of the three-dimensional grid point p_j and the charge amount $dval_j$ of the point are combined to form a meshed interpolation matrix.

ANALYSIS AND RESULTS

Comparison of Algorithm before and After Improvements

Taking a simple three-dimensional model as an example, as shown in Figure 4(a), the simple three-dimensional model is established as follows: a charged sphere with a radius of 0.6m is placed in a semi-infinite space. The center coordinates of the sphere are (0.5, 0.5, -1). The surface of the semi-infinite space is at Z=0m. The volume charge density of the sphere is 1C/m^3. The surface potential distribution at Z=0m is shown in Figure 4(b).

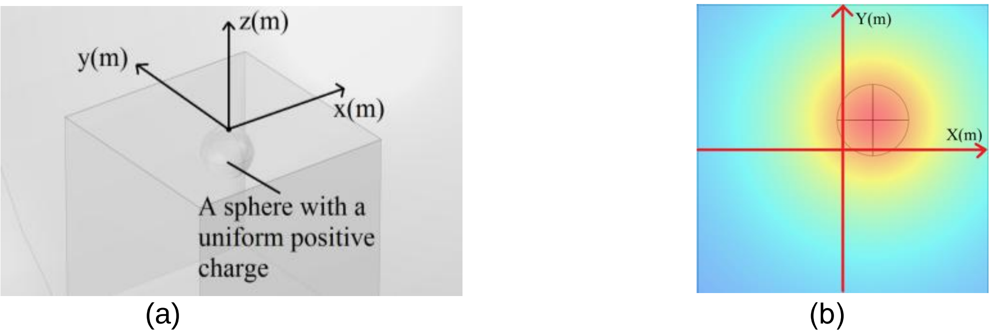

(a) (b)

Fig. 4 - Surface potential distribution at z = 0m

The standard particle swarm algorithm and the improved particle swarm algorithm are respectively used for inversion test, as shown in Figures 5 to 6. The direction of each axis of the coordinate system in Figures 5 to 6 is consistent with the direction of each axis of the coordinate system in Figure 4, but the coordinate origin in Figures 5 to 6 is located at (0, 0, -2) in the coordinate system of Figure 4.

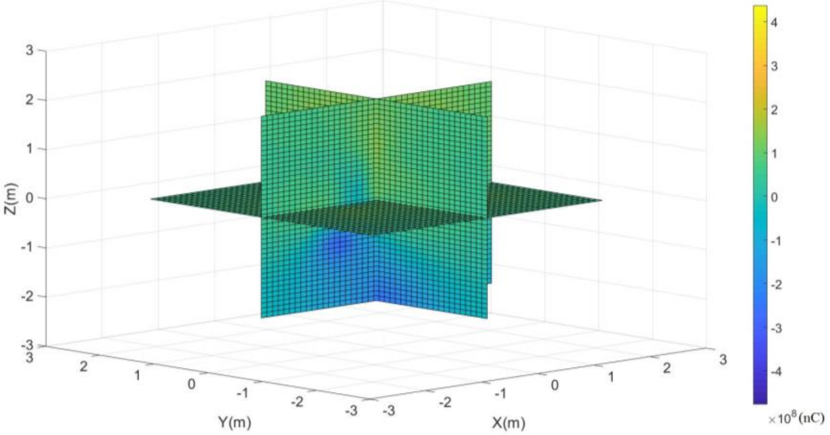

Fig.5 - Inversion result diagram of standard particle swarm optimization algorithm

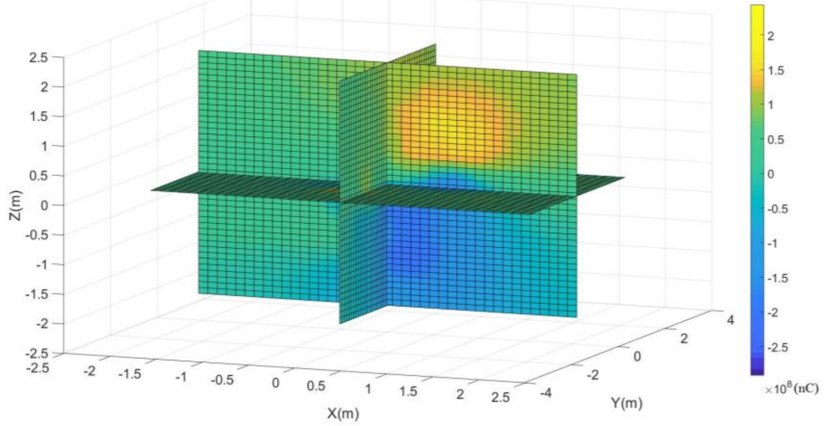

Fig.6 - Inversion Results of Improved Particle Swarm Optimization Algorithm

The convergence curves of the algorithms are shown in Figure 7.

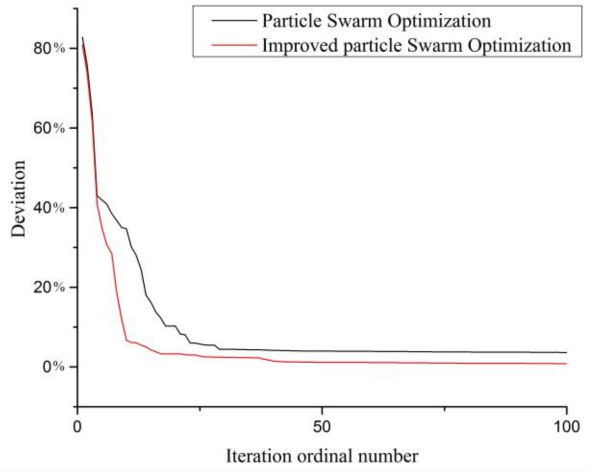

Fig. 7 Convergence curve of algorithm

As shown in Figure 7, the inversion fitting variance of the improved PSO algorithm is significantly smaller than that of the standard PSO algorithm. Compared with the standard PSO algorithm, the inversion results of the improved PSO algorithm match the established model to a better extent, which shows better inversion effect.

Forward Simulation Data Inversion

The basic steps of the algorithm are as follows:

(1) Import raw data and set inversion parameters;
(2) Apply adaptive outlier filtering to preprocess the original data and remove outliers;
(3) Use the adaptive weighted particle swarm optimization algorithm to invert the preprocessed data;
(4) When optimization stagnates, apply chaos mapping to the optimal solution to expand the search range;
(5) Stop iteration when the objective fitness is reached, and apply adaptive outlier filtering to the discrete point cloud to make the results conform more to geological laws;
(6) Export the data and create plots.

Taking the aforementioned three-dimensional coupled model of seepage field-natural electric field as an example, the inverse processing of the forward data is carried out in the following steps:

(1) As shown in Figure 3, the potential distribution of the surrounding tunnel wall is obtained on the tunnel wall of the forward model centered on the seepage point;
(2) Establish a square with a side length of 2 m as the inversion area, and take the center of the inversion area as the origin to establish a three-dimensional coordinate system, in which the Z-axis points beyond the inner wall of the tunnel, the Y-axis is upward, and the X-axis is to the right, so that the coordinates of the inner wall of the tunnel are Z=1 m, and the coordinates of the water seepage point are (0, 0, 1). The established coordinate system is shown in Figure 8.
(3) Inversion parameter setting: a target fitting variance of 1%; a maximum number of iterations of200, and an initial filtering parameter-filtering number of1.

In this inversion trial, the variance of the inversion results from the forward data is 1.58%. The inversion results are shown in Figure 8.

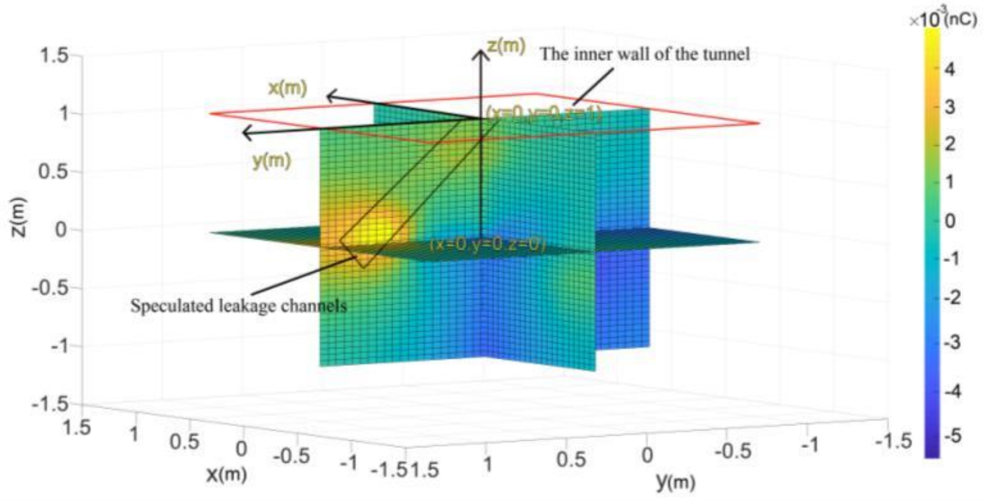

Fig. 8 - Inversion Results of Forward Model

It can be seen from Figure 8 of the inversion results that the position and morphology of the leakage channel in the forward model have a good correspondence with the position and morphology of the positive charge concentration distribution in the space charge inversion result diagram. Therefore, the spatial charge distribution inversion based on the forward data is reliable.

Inversion Study of Measured Data

After long-term operation, water seepage occurs in the inner wall of a tunnel, and it is necessary to carry out leakage plugging construction on the seepage channel. Taking the seepage location of the tunnel as an example, the effectiveness of the detection method is further verified. As shown in Figure 9(a), the measuring points are arranged where water seepage occurs in the tunnel inner wall, and the distribution of measuring points is depicted as shown in Figure 9(b).

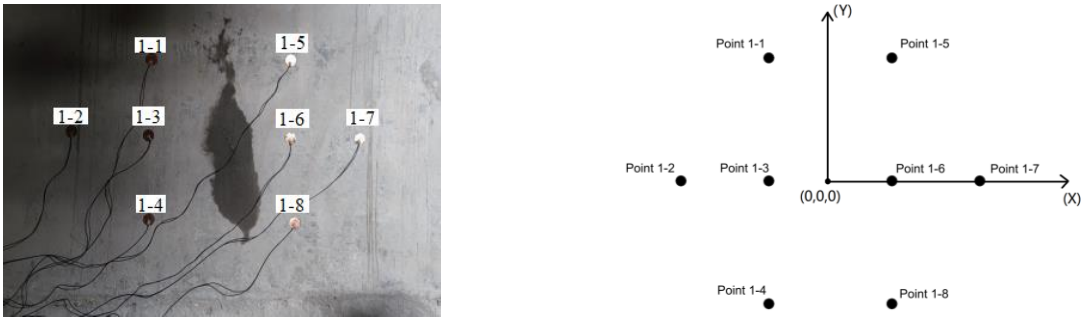

(a) (b)

Fig.9 - Layout of Measuring Points for Measured Data

Based on the distribution of the measured points, a spatial coordinate system with the X and Y axes is established, as shown in Figure 9(b). The seepage point is the origin of the X-Y axis coordinate system. The Z-axis is set to point outward from the tunnel surface, where the Z-axis coordinate of the tunnel surface is 2m. Therefore, the origin of the coordinate system is 2m inside the tunnel lining, located at the intersection of the X and Y axes. Table 1 shows the coordinates and potential values of each measured point, and Figure 10 shows the potential distribution on the inner wall surface of the tunnel (interpolated using the Kriging method).

Tab. 1 - Measured Point Coordinates and Potential Values

Dot	X	Y	Z	potential(mV)
Point 1-1	-0.35	0.7	2	-14.8082
Point 1-2	-0.85	0	2	25.7779
Point 1-3	-0.35	0	2	27.4132
Point 1-4	-0.35	-0.7	2	5.4714
Point 1-5	0.35	0.7	2	-27.6113
Point 1-6	0.35	0	2	-32.2695
Point 1-7	0.85	0	2	1.4756
Point 1-8	0.35	-0.7	2	-27.3133

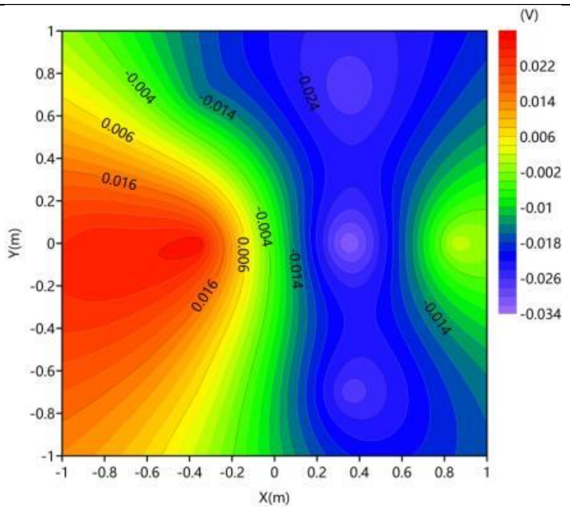

Fig. 10 Potential distribution of inner wall surface of tunnel

The inversion process utilizes parameters such as a target fitting variance of 5%, maximum iteration times of 200 and initial filtering parameters - filtering times of 1. The inversion variance is 7.6%. The inversion result is shown in Figure11.

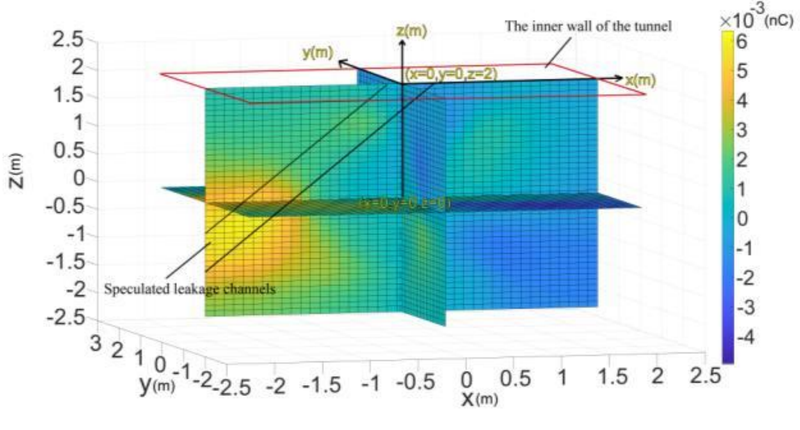

Fig.11 Inversion Results of Measured Data

From the inversion result in Figure11, it can be observed that the spatial charge distribution inversion based on the measured data corresponds to the actual situation of charge anomaly distribution caused by leakage channels. It can be inferred that the leakage channels in the external surrounding rock of the tunnel lining may exist at the location surrounded by the black wireframe in Figure 11. During the excavation process of the circled seepage channel, the excavation results showed that at the abnormal position shown in Figure 11, the soil was loose and water seepage occurred. The loose part was excavated and replaced, and after treatment, there was no water seepage.

CONCLUSION

The following points can be drawn:

(1) When there are leakage channels in the tunnel lining and the external surrounding rock, the potential distribution on the inner surface of the tunnel lining near the leakage channels will be significantly affected by the flow potential, resulting in anomalies.

(2) The inversion software based on the improved chaos particle swarm optimization algorithm achieves a variance of 1.58% in the inversion of the forward model and a variance of 7.6% in the inversion of the measured data. Moreover, the charge anomaly distribution areas in the inversion results of the forward model are well correlated with the locations of leakage channels in the established model. In the inversion of the measured data, the distribution of charge anomalies conforms to geological laws. Therefore, the improved chaos PSO algorithm demonstrates good convergence and high consistency in the inversion of three-dimensional spatial charge distributions.

(3) Through the analysis of the inversion results of numerical simulation data and measurement data, it can be seen that the improved chaotic PSO algorithm is used to perform three-dimensional inversion of the leakage channel inside the tunnel surrounding rock using the potential distribution of the tunnel lining layer as the original data, which is consistent with the actual situation. The inversion algorithm has high reliability.

REFERENCES

[1] Fu, J.K. 2012. Study on the causes of water leakage and its impact on structures of highway tunnel [D]. Southwest Jiaotong University.

[2] Yao, Z.Z., Yang, C.P. 2014. Rectification measures for leakage water leakage in tunnels in active operation of expressways (in Chinese). Transportation Science & Technology, no. 02, pp. 112-115.

[3] Hunter, R. J. 2013. Zeta Potential in Colloid Science: Principles and Applications. Academic Press.

[4] Chenyakin, Y., & Chen, D. D. Y. 2021. Characterization of capillary inner surface conditions with streaming potential. Electrophoresis, vol. 42, no. 20, pp. 2094-2102. https://doi.org/10.1002/elps.202100167

[5] Siani, P., Frigerio, G., Donadoni, E., & Di Valentin, C. 2023. Modeling Zeta Potential for Nanoparticles in Solution: Water Flexibility Matters. The Journal of Physical Chemistry C, vol. 127, no. 19, pp. 9236-9247. https://doi.org/10.1021/acs.jpcc.2c08988

[6] Hamlyn, J., Cottrell, R. J., Bird, C. L., & Kulessa, B. 2023. Observing water flow within an embankment dam using self-potential monitoring. Dams and Reservoirs, vol. 33, no. 1, pp. 19-26. https://doi.org/10.1680/jdare.22.00085

[7] Bolève, A., Vandemeulebrouck, J., & Grangeon, J. 2012. Dyke leakage localization and hydraulic permeability estimation through self-potential and hydro-acoustic measurements: Self-potential 'abacus' diagram for hydraulic permeability estimation and uncertainty computation. Journal of Applied Geophysics, vol. 86, pp. 17-28. https://doi.org/10.1016/j.jappgeo.2012.07.007

[8] Kukemilks, K., & Wagner, J. F. 2021. Detection of Preferential Water Flow by Electrical Resistivity Tomography and Self-Potential Method. Applied Sciences, vol. 11, no. 9, pp. 4224. https://doi.org/10.3390/app11094224

[9] Wang, Y., Chung, E., & Sun, S. 2022. Physics-preserving IMPES based multiscale methods for immiscible two-phase flow in highly heterogeneous porous media. arXiv preprint arXiv:2212.05942. https://doi.org/10.48550/arXiv.2212.05942

[10] Xu, R. 2023. Stability of surrounding rock in broken zone of the tunnel in rich water and mountains. Desalination and Water Treatment, vol. 290, pp. 170-176. Doi: 10.5004/dwt.2023.29419

[11] Gambolati, G., & Freeze, R. A. 1973. Mathematical simulation of the subsidence of Venice: 1. Theory. Water Resources Research, vol. 9, no. 3, pp. 721-733. https://doi.org/10.1029/WR009i003p00721

[12] Li, B. 2023. A Productivity Prediction Method Based on Artificial Neural Networks and Particle Swarm Optimization for Shale-Gas Horizontal Wells. Fluid Dynamics & Materials Processing, vol. 19, no. 10, pp. 2729-2748. DOI:10.32604/fdmp.2023.029649

[13] Chatterjee, A., & Siarry, P. 2006. Nonlinear inertia weight variation for dynamic adaptation in particle swarm optimization. Computers & Operations Research, vol. 33, no. 3, pp. 859-871. https://doi.org/10.1016/j.cor.2004.08.012

[14] Abualigah, L., Almotairi, K. H., AbdElaziz, M., Shehab, M., & Altalhi, M. 2022. Enhanced Flow Direction Arithmetic Optimization Algorithm for mathematical optimization problems with applications of data clustering. Engineering Analysis with Boundary Elements, vol. 138, pp. 13-29. https://doi.org/10.1016/j.enganabound.2022.01.014

[15] Shi, K., Cai, Y.G., Zou, G.S., Wang, T. 2005. Comparison between Ant Colony Algorithm and Particle Swarm Optimization and their application in VRP. Proceeding of the 24th Chinese Control Conference, Guangzhou, China, pp. 732-735.

[16] Li, H. 2010. Inverse Problems of Partial Differential Equations Particle Swarm Algorithm [D]. Xi’an University of Technology.

[17] Zou, S., Ji, J.M., Yang, X.D., He, Y.M. 2021. Application of Improved PSO Algorithm in Reactive Power Optimization of Power System. Information & Computer, vol. 33, no. 24, pp. 77-80.

[18] Altinoz, O. T., Yilmaz, A. E., & Weber, G. W. 2010. Chaos Particle Swarm Optimized PID Controller for the Inverted Pendulum System. 2nd international conference on engineering optimization, Lisbon, Portugal.

[19] Kennedy, J., & Eberhart, R. 1995. Particle Swarm Optimization. Proceedings of ICNN'95 - International Conference on Neural Networks, Perth, WA, Australia, IEEE, vol. 4, pp. 1942-1948. DOI: 10.1109/ICNN.1995.488968

[20] El Rassy, E., Delaroque, A., Sambou, P., Chakravarty, H. K., & Matynia, A. 2021. On the Potential of the Particle Swarm Algorithm for the Optimization of Detailed Kinetic Mechanisms. Comparison with the Genetic Algorithm. The Journal of Physical Chemistry A, vol. 125, no. 23, pp. 5180-5189. https://doi.org/10.1021/acs.jpca.1c02095

[21] Dong, W. Y., & Zhang, R. R. 2022. Stochastic stability analysis of composite dynamic system for particle swarm optimization. Information Sciences, vol. 592, pp. 227-243. https://doi.org/10.1016/j.ins.2021.12.095

[22] Wang, S., Liu, Y., Zou, K., Li, N., & Wu, Y. 2022. Multiobjective Particle Swarm Optimization Based on Ideal Distance. Discrete Dynamics in Nature and Society, vol. 2022, pp. 3515566. https://doi.org/10.1155/2022/3515566

[23] Li, R., Yu, N., Li, R., Zhuang, Q., & Zhang, H. 2021. Transient electromagnetic inversion based on particle swarm optimization and differential evolution algorithm. Near Surface Geophysics, vol. 19, no. 1, pp. 59-71. https://doi.org/10.1002/nsg.12129

[24] Zhang, J., Sun, Z., Qiu, N., Zhang, Y., & Li, F. 2019. 3-D effetive elastic thickness inversion of subduction zone based on particle swarm optimization algorithm. Chinese Journal of Geophysics, vol. 62, no. 12, pp. 4738-4749.Doi: 10.6038/cjg2019M0247

[25] Wardhana, S. G., & Pranowo, W. 2022. Rock-physics modeling by using particle swarm optimization algorithm. Journal of Applied Geophysics, vol. 202, pp. 104683. https://doi.org/10.1016/j.jappgeo.2022.104683

[26] Liu, B., Wang, L., Jin, Y. H., Tang, F., & Huang, D. X. 2005. Improved particle swarm optimization combined with chaos. Chaos, Solitons & Fractals, vol. 25, no. 5, pp. 1261-1271. https://doi.org/10.1016/j.chaos.2004.11.095

[27] Zeedan, M., Attiya, G., & El-Fishawy, N. 2022. A Hybrid Approach for Task Scheduling Based Particle Swarm and Chaotic Strategies in Cloud Computing Environment. Parallel Processing Letters, vol. 32, no. 01n02, pp. 2250001. DOI:10.1142/S0129626422500013

[28] Gao, S., Yang, J.Y. 2006. Research on Chaos Particle Swarm Optimization Algorithm. Pattern Recognition

and Artificial Intelligence, vol. 19, no. 02, pp. 266-270.

[29] Yang, J.J., Zhou, J.Z., Yu, J., Wu, W. 2005. Particle swarm optimization algorithm based on chaos searching. Computer Engineering and Applications, no. 16, pp. 69-71.